Numerical simulation of shrinkage and warpage deformation of an intermittent-extrusion blow molded part: validation case study

Benrabah, Z.; Bardetti, A.; Ilinca, F.; Ward, G.

Publisher's version / Version de l'éditeur:

ANTECH 2018 Conference Proceedings, 2018

NUMERICAL SIMULATION OF SHRINKAGE AND WARPAGE DEFORMATION OF AN INTERMITTENT-EXTRUSION BLOW MOLDED PART: VALIDATION CASE STUDY

Z. Benrabah[1], A. Bardetti[1], F. Ilinca[1], G. Ward[2]

[1]National Research Council Canada – Automotive and Surface Transportation Research Center, 75 de Mortagne Blvd., Boucherville, Québec J4B 6Y4, Canada
[2]Agri-Industrial Plastics Company, 301 North 22nd Street – Fairfield, IA 52556, USA

Abstract

Intermittent extrusion blow molding is increasingly being used in polymer forming processes for the production of complex thermoplastic industrial parts with short cycle times. During this process residual stresses caused by inhomogeneous cooling and relaxation of polymer chains, often result in shrinkage and warpage of the final part. One challenging quality requirement of industrial blow molded parts is geometric tolerances. Therefore part deformation, due to cooling and solidification, needs to be controlled and optimized according to specific design criteria. In particular, the complex design shapes of plastic fuel tank (PFT) shells exacerbate these challenges which need to be resolved upfront, in the early stages of product development and tool design. Consequently, the development of an accurate simulation tool, well suited for industrial applications, to predict thermoplastic part deformations due to cooling and solidification, has become essential for part designers to help achieve an efficient production with minimum manufacturing cost.

The aim of this work is to present the latest advancements in predicting the shrinkage and warpage deformation of a curved PFT, designed for agricultural machinery, using NRC's BlowView[1] software. This case study validation considers the entire blow molding stages (i.e., polymer flow in the die, parison formation, inflation, and finally in and out of mold cooling during part solidification). The simulation results, in terms of thickness distribution and displacements, are compared to an actual scanned part using the best fit technique in order to exemplify the accuracy and reliability of the modelling approach.

[1] BlowView is an engineering simulation software package developed at NRC capable of simulating and optimizing extrusion blow molding, stretch blow molding and thermoforming processes [1-6].

Introduction

Nowadays, the thermoplastic forming market is expanding to more complex geometries and uses a large array of materials. Since thermoplastic forming processes are highly automated, they are predestined for large-scale manufacturing. Part designers are under increasing pressure to reduce development time and manufacturing costs, while ensuring maximum part quality (better, faster, cheaper). The success of a part development phase depends on many technical aspects such as; part development time, amount of rework, process set-up times and tooling costs. All these aspects must be considered and well understood by designers in order to find the optimal processing parameters, mold design and cooling conditions in order to satisfy all part specifications. Particular attention must also be given to the warpage and shrinkage deformation that occurs during the cooling and solidification phase. This aspect becomes a decisive quality criterion for part acceptance, especially for PFT manufactures where tolerance issues are so critical. Indeed, during the part cooling phase, residual stresses caused by inhomogeneous cooling and relaxation of polymer chains, often result in shrinkage and warpage deformation of the final part. It is not surprising to see a part either break once it is ejected from the mold, or distort and twist after a couple of days in the warehouse, even though it initially had the desired shape [1-6]. Therefore, the accurate prediction of part deformation due to solidification is an important aspect to be addressed and controlled in order to permit design teams to achieve an efficient product development phase.

In this article, a numerical model for the prediction of thermally induced stresses and the resulting shrinkage and warpage during solidification is studied. First, the thermal model used for computing the temperature field of formed parts is presented. Thereafter, special emphasis is placed on the viscoelastic constitutive model and its recurrent formulae used for incremental calculation of time-dependent residual stresses. The warpage deformation of the part, based on a thermo-

viscoelastic model, is finally derived for small strains formulation under small displacement theory [5].

To conclude, a finite element analysis based on this formulation, is performed on a validation case study that deals with a complex curved industrial PFT. The comparison with experimental results in terms of thickness distribution at the end of the extrusion and inflation stages is discussed and presented. In order to assess part shrinkage and warpage during solidification, the simulation results are compared with experimental measurements on an actual scanned part, in terms of the normal distance, using the best fit technique. The material considered for the study is Marlex® HXM 50100 HDPE blow molding grade. The material properties required for the simulation are obtained using standard tests for specific heat, density, thermal conductivity and relaxation spectrum at molten and solid states (for inflation and warpage).

THEORETICAL APPROACH

Thermal Model

Given the inherent low thermal conductivity of plastics, and the special geometrical configuration of the formed part (i.e., relatively thin compared to the surface area), unilateral cooling is usually assumed to be a one dimensional transient heat conduction problem through the part thickness [4-6]. Taking into account the effect of heat absorption due to crystallization of the polymer during the cooling stage leads to the following heat balance equation:

$$\rho C_p \frac{\partial T}{\partial t} = \frac{\partial}{\partial x}\left(k \frac{\partial T}{\partial x}\right) + \dot{Q}_{Cry} \qquad (1)$$

where ρ, C_p and k are the density, specific heat and thermal conductivity of the polymer respectively that may be considered constant or temperature dependent [3, 4], T is the temperature and t is the elapsed time. The $\dot{Q}_{Cry}$ term describes the volumetric heat absorption due to crystallization.

The solution of the balance energy equation (1) depends on the initial temperature and on the boundary conditions (2)-(5). As initial conditions for the cooling stage, we use the final temperature field provided at the end of the forming stage. It is then assumed that the energy interchange between the outer surface of the part and the surface of the mold before demolding, and surrounding air after demolding, occurs by free convection. The energy interchange between the inner surface and cavity air also occurs by lateral free convection. The boundary conditions on the inner and outer surface of the part before demolding and after demolding are given as follows:

$$-k \frac{\partial T}{\partial x} = h_{Air}^{Part} . \left(T_s^{in} - T_{Air}^{in}\right) \qquad (2)$$

$$-k \frac{\partial T}{\partial x} = h_{Mold}^{Part} . \left(T_s^{out} - T_{Mold}\right) \qquad (3)$$

$$-k \frac{\partial T}{\partial x} = h_{Air}^{Part} . \left(T_s^{in} - T_{Air}^{in}\right) \qquad (4)$$

$$-k \frac{\partial T}{\partial x} = h_{Air}^{Part} . \left(T_s^{out} - T_{Air}^{out}\right) \qquad (5)$$

where h_{Air}^{Part} and h_{Mold}^{Part} are the convection coefficients between the surface of the part and the air, and the surface of the part and the mold, respectively. They may be considered constant or, more realistically, variable with time and position [2]. T_s^{in} and T_s^{out} are the inner and outer surface temperature of the part, respectively. T_{Air}^{in} and T_{Air}^{out} are the inner and the outer air temperature and T_{mold} is the mold temperature. The crystallization heat absorption $\dot{Q}_{Cry}$ term is given by the following expression [7-8]:

$$\dot{Q}_{Cry} = \left(\rho \Delta H_{Cry}\right) . \frac{\partial \chi(t)}{\partial t} \qquad (6)$$

where ΔH_{Cry} is the latent heat of crystallization and χ is the relative degree of crystallinity. According to [7- 9], the Nakamura model is a well-known model for the prediction of crystallinity during polymer processing. The model is a differential expression that gives the rate of crystallization $\frac{\partial \chi}{\partial t}$ as a function of the temperature T:

$$\frac{\partial \chi}{\partial t} = nK(T)(1-\chi) . \left[ln\left(\frac{1}{1-\chi}\right)\right]^{\left(\frac{n-1}{n}\right)} \qquad (7)$$

Where n is the Avrami exponent and $K(T)$ is the temperature dependent rate constant parameter given by the Hoffman-Lauritzen theory through the following expression:

$$K(T) = K_0 exp\left(\frac{U}{R\left(T - T_g + 30\right)}\right) - \frac{C(T + T_m)}{2T^2(T_m - T)} \qquad (8)$$

where K_0 is the model constant, U the activation energy, R is the universal gas constant, C is the nucleation exponent, T_g is the glass transition temperature and T_m is the melting temperature. The partial differential equation (1) and the set of boundary conditions (2)-(5) describing such a problem is often referred to as the strong form. The differential equations may be either linear or nonlinear. Consequently, the exact analytical

solutions of the heat transfer governing equations can only be obtained for problems in which restrictive simplifying assumptions are made with respect to geometry, material properties and boundary conditions. There is therefore, no option but to turn to numerical solution methods for the analysis of practical problems, where such simplifications are generally not possible.

Thermal Finite Element Discretization

Based on the Galerkin approximation method and combining the balance equation (1) and the boundary conditions (2)-(5), it is simple to show that the previous thermal problem is reduced to the following compact matrix form [10]:

$$[C(T)]\{\dot{T}\} + [K(T)]\{T\} = \{F(T)\} \quad (9)$$

in which,

$\{T\} = \{\boldsymbol{T_n}\}$;

$$C_{ij} = \int_{\Omega} \left(N_i . \rho C_p(T) . N_j\right) d\Omega$$

$$K_{ij} = \int_{\Omega} \left(\frac{\partial N_i}{\partial x} k(T) . \frac{\partial N_j}{\partial x}\right) d\Omega + \int_{\Gamma_{\text{Mold}}} \left(N_i . h_{Mold}^{Part} . N_j\right) d\Gamma + \int_{\Gamma_{\text{in}}} \left(N_i . h_{Air}^{Part} . N_j\right) d\Gamma + \int_{\Gamma_{\text{out}}} \left(N_i . h_{Air}^{Part} . N_j\right) d\Gamma$$

$$F_i = \int_{\Omega} \left(N_i . \rho \Delta H_{Cry} . \frac{\partial \chi}{\partial t}\right) d\Omega + \int_{\Gamma_{\text{Mold}}} (N_i . h_{Mold}^{Part} . T_{Mold}) d\Gamma + \int_{\Gamma_{\text{in}}} \left(N_i . h_{Mold}^{Part} . T_{air}^{in}\right) d\Gamma + \int_{\Gamma_{\text{out}}} (N_i . h_{Air}^{Part} . T_{Air}^{out}) d\Gamma$$

Where, the component of vector T_n are the nodal temperatures and N_i are the element shape functions. For the transient case under consideration, the global capacitance [C] and conductance matrices [K] are temperature dependent. The non-linearity is due to the temperature dependent thermal conductivity, density, specific heat, and non-isothermal crystallization kinetics. Since [C], [K], and {F} may strongly depend on the unknown temperature, the system of equations (9) may be strongly nonlinear. Also, Ω is the initial volume of the deformable thermoplastic continuous body (parison and/or sheet) and Γ is the surface boundary of this volume. Γ_{in} and Γ_{out} are respectively, the inner side and the outer side of the surface Γ, that are in contact with air. Γ_{Mold} is the part surface that is in contact with the mold.

Forming Deformation Model

In thermoplastic forming processes, the initial deformable thermoplastic body is geometrically completely defined. Therefore, a total Lagrangian formulation with the reference configuration as the initial undeformed configuration is adopted. Since most of the final products in thermoplastic forming processes consist of thin walled structures, in this paper we assume that the thermoplastic material is modeled as a two-dimensional thin membrane structure [5]. Based on the principal of stationary potential energy, we know that the total energy Π of a deformable body submitted to external loads tends to a minimum with regards to the displacement, which is expressed as [10]:

$$\delta\Pi = \delta\Pi_{\text{int}} - \delta w_{\text{ext}} = 0 \quad (10)$$

Where $\delta\Pi_{\text{int}}$ is the variation of strain energy of the deformable body and δw_{ext} is the variation of the work of external forces. In Lagrangian formulation, the variation of the strain energy can be expressed as a function of the 2nd Piola-Kirchoff stress tensor *S* and the conjugated Green-Lagrange strain tensor *E* as follows:

$$\delta\Pi_{\text{int}} = \int_{\Omega} \delta E^{\text{T}} . S \ \text{d}\Omega \quad (11)$$

where Ω is initial volume of the deformable thermoplastic body. The variation of the work of external forces is given by the following expression:

$$\delta w_{\text{ext}} = \int_{\Omega} \delta \boldsymbol{u}^{\text{T}} . f_{\text{v}} \text{d}\Omega + \int_{\Gamma} \delta \boldsymbol{u}^{\text{T}} . f_{\text{s}} \text{d}\Gamma \quad (12)$$

where f_{v} is body volume force vector and f_{s} is external surface force vector applied on the external body surface *Γ*. $\delta \boldsymbol{u}^{\text{T}}$ is the transposed virtual displacement vector, that is compatible with displacement boundary conditions.

Constitutive model implementation

The KBK-Z rheological model used to describe the multilayer viscoelastic deformations that occur during polymer forming processes, i.e., stress (*S*)–strain (*E*) relationship used in equation (11). This model is well known to adequately represent polymer behaviour at the molten state [11, 12]. For this model, the true stress σ (Cauchy stress) tensor at time *t* is related to the history

of Finger deformation tensor $B(t,t')$ and to the right Cauchy-Green deformation tensor $C(t,t')$ according to:

$$\sigma_{ij}(t) = -p\bar{I} + \left(\frac{1}{1-\theta}\right).\int_{-\infty}^{t}\left[\sum_{k=1}^{n}\frac{G_k}{\lambda_k}e^{-\left(\frac{t-t'}{\lambda_k}\right)} \cdot h(I_1,I_2) \cdot \left(B_{ij}(t,t') - \theta.C_{ij}(t,t')\right)\right]dt \quad (13)$$

where p is the iso-static pressure; λ_k and G_k are the relaxation time and relaxation modulus coefficient, respectively. $h(I_1,I_2)$ is the damping function known as PSM model introduced by Papanastasiou et *al* [13].

$$h(I_1,I_2) = \frac{\alpha}{(\alpha-3)+\beta I_1+(1-\beta)I_2} \quad (14)$$

I_1 and $I_2$are the first and the second invariants of the finger stain tensor. α and β are material dependant coefficient. Finger deformation tensor $B(t,t')$ is related to the right Cauchy-Green deformation tensor $C(t,t')$ by:

$$B_{ij}(t,t') = C_{ij}^{-1}(t,t') = \left[F_{ij}^{T}F_{ij}\right]^{-1} \quad (15)$$

Where F_{ij} is the material deformation gradient tensor defined from the displacement field $\boldsymbol{u}(\boldsymbol{X},t)$ generated by the movement of the point $\boldsymbol{P}$. The displacement is expressed in terms of material coordinates as:

$$\boldsymbol{u}(\boldsymbol{X},t) = \boldsymbol{x}(\boldsymbol{X},t) - \boldsymbol{X} \quad (16)$$

With $\boldsymbol{X}$ being the position of point $\boldsymbol{P}$ in the undeformed configuration and $\boldsymbol{x}$ the position of the same point in the deformed configuration. The deformation gradient F has the following matrix form in membrane formulation:

$$F^{\mathrm{T}} = \begin{bmatrix} x_{,X} & x_{,Y} & 0 \\ y_{,X} & y_{,Y} & 0 \\ z_{,X} & z_{,Y} & 0 \end{bmatrix} \quad (17)$$

Since we are dealing with a thin membrane element, we assume in this paper a plane stress state. Therefore the components of Cauchy stress tensors have the following properties:

$$\sigma_{13} = \sigma_{23} = \sigma_{31} = \sigma_{32} = \sigma_{33} = 0 \quad (18)$$

In Lagrangian formulation the 2nd Piola–Kirchhoff stress tensor (S_{ij}) relates forces in the reference configuration to its areas in the reference configuration. This stress could be related to the Cauchy stress by the following standard equation:

$$S_{ij}(t) = J(t).F^{-1}(t)\,\sigma(t)F^{-T}(t) \quad (19)$$

Where J(t) is the jacobian transformation. Since the polymeric material is considered as incompressible isotropic materials, the jacobian is unity:

$$J(t) = \det(F) = 1 \quad (20)$$

The process induced residual stress tensor $S(t)$ at the end of the inflation will be used as the initial stress in warpage analysis.

Temperature dependence

The WLF equation incorporates the temperature dependence of the material properties through the following relationship, the shift factor $a(T)$ being subsequently applied to the relaxation time and the relaxation modulus as follows [14]:

$$\lambda_k = a(T).\lambda_k^{ref} \quad (21)$$

Where subscript 'ref' denotes the reference state. T_{Ref} and T are the reference and absolute Temperatures respectively; and $a(T)$ represents the shift factor given by:

$$ln\big(a(T)\big) = \frac{C_1\big(T - T_{Ref}\big)}{C_2 + T - T_{Ref}} \quad (22)$$

It is important to note that T is the temperature obtained from the previously presented thermal model; C_1 and C_2 are material constants. The numerical results obtained from the forming processes (mainly thickness and temperature distribution) are the basis for the subsequent calculation of shrinkage and warpage deformations.

Shrinkage and Warpage Deformation Model

Once the polymeric parison melt is inflated inside the cavity, it rapidly cools down and solidifies until it has enough strength to be taken out of the mold for additional cooling in ambient air. While in the mold, thermal stresses start developing due to non-uniform wall thickness and temperature profiles. After demolding, formed parts undergo shrinkage and warpage caused by accumulated thermal stresses, additional mechanical stresses and out of mold temperature evolution. Small induced deformations are often observed on warped parts. Considering this deformation magnitude, a linear deformation approach is usually well adapted and gives adequate results. Based on generalized N elements Maxwell model, the stress relaxation function is given by [15]:

$$\sigma(t) = \sum_{k=1}^{N} g_k \, e^{-\left(\frac{t}{\tau_k}\right)} \times \varepsilon_0 \qquad (23)$$

Where g_k and τ_k are the spectra of elastic modulus and relaxation times of the polymer at solid state, respectively and ε_0 is the constant deformation step applied to the sample. The development of a numerical model based on the general integral representation of linear viscoelasticity, assuming that the cooling polymer behaves as an isotropic thermo-rheological simple solid, is well presented in paper [15], and we recall here only the main derived equations for multilayer materials. The residual stresses in the material layer L at time step t_{n+1} are obtained from the stresses and deformations at time step t_n according to:

$$\sigma_{ij,L}^{n+1} = \sum_{k=1}^{N} \bar{g}_{k,L} \sigma_{ij,L}^{k,n+1} \qquad (24)$$

where

$$\sigma_{ij,L}^{k,n+1} = \left(\sigma_{ij,L}^{k,n}\right) e^{-\left(\frac{t_{n+1}-t_n}{\tau_{k,L}}\right)} + \left[[H_L]\Delta\varepsilon_{ij,L}^{n} - \Delta{\sigma_{ij,L}^{th}}^{n}\right]\left[\frac{\tau_{k,L}}{t_{n+1}-t_n}\left(1 - e^{-\left(\frac{t_{n+1}-t_n}{\tau_{k,L}}\right)}\right)\right] \qquad (25)$$

and $\sigma_{ij,L}^{k,o} = \sigma_{ij,L}^{0}$; $\sigma_{ij,L}^{0}$ represent the residual process induced stresses at the beginning of the in-mold cooling stage. For intermittent extrusion blow molding processes, the in-mold thermally induced stresses should be superposed to the residual induced stresses given by equation (13) at the end of inflation stage. $\Delta\varepsilon_{ij,L}^{n} = \varepsilon_{ij,L}^{n+1} - \varepsilon_{ij,L}^{n}$. $[H_L]$ is the plane stress elastic matrix containing the material elastic coefficients of the layer L at time $t = 0$, ε represents the strain tensor (small displacement theory), $\bar{g}_{k,L}$ and $\tau_{k,L}$ are the spectra of normalized elastic modulus and relaxation times of the polymer for layer L at solid state, respectively. ${\sigma_{ij,L}^{th}}^{n}$ are the thermal stresses at time t_n defined by [15; 16]:

$${\sigma_{ij,L}^{th}}^{n} = \frac{-E(t)}{3.(1-\nu)} \times \frac{\alpha\left(T_{t_{n+1}}\right) + \alpha\left(T_{t_n}\right)}{2} \times \left(T_{t_{n+1}} - T_{t_n}\right)\delta_{ij} \qquad (26)$$

where $\alpha(t)$ is the material's dilatation coefficient. The modulus E(t) is given by a Maxwell-Weichert viscoelastic model with six relaxation times:

$$E(t) = \sum_{k=1}^{n} g_k \, e^{-\left(\frac{t}{\tau_k}\right)} \qquad (27)$$

The finite element implementation is based on the methodology presented in [5].

Validation Case Study

The part considered for the validation is a large, complex, curved, monolayer PFT shown in Figure 1. Marlex® HXM 50100 HDPE blow-molding grade is considered for this study and its material properties are summarized in Table 1**Error! Reference source not found.**. It is characterized using standard tests for specific heat, density, thermal conductivity, and relaxation spectrum at molten and solid states, covering the entire temperature range from extrusion to solidification. The thermal expansion coefficients, derived from the material's PVT data, must also be accurately determined to simulate warpage.

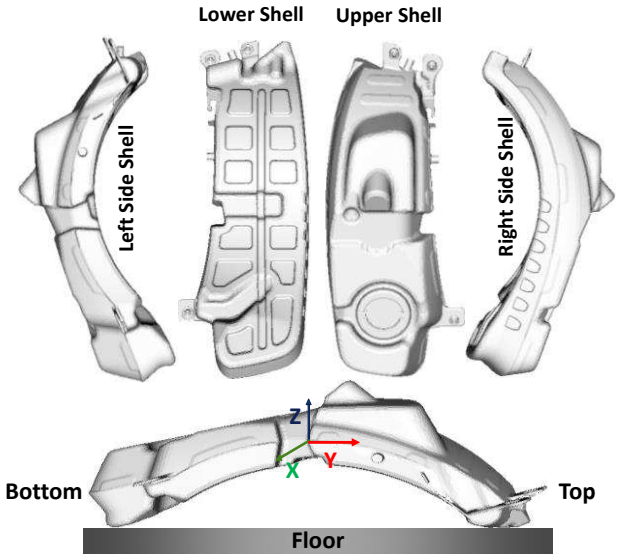

Figure 1: Blow molded PFT from Agri-Industrial Plastics Company

The BlowView simulation considers the entire blow molding process stages from parison extrusion, mold clamping and inflation, to solidification. The cooling is performed in two steps: the first is in the mold, where the part is confined and cannot deform freely due to boundary conditions, and the second is outside the mold, once the part is ejected and can deform freely. Based on the processing conditions listed in Table 2, the parison formation, accounting for swell, sag and non-isothermal effects, was predicted using the BlowParison [17, 18] module, provided with the BlowView software package. The parison shape and thickness distribution at the end of the extrusion and pre-blow stages are depicted in Figure 2a) and 2b), respectively.

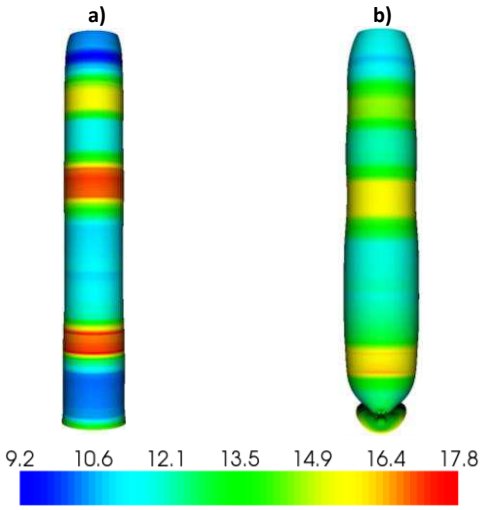

Figure 2: Parison formation and thickness distribution (mm) at the: a) end of extrusion; b) end of pre-blow

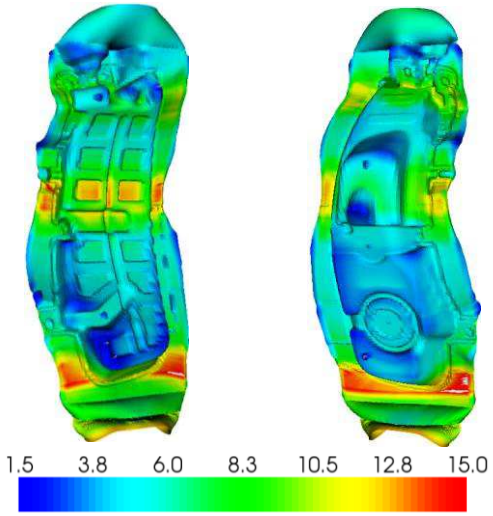

Figure 3: Thickness distribution (mm) of inflated parison

The predicted thickness distribution at the end of the inflation, prior to cooling in-mold, is shown in Figure 3. In order to compare the simulation results to measured values, the predicted thickness distribution, at the end of the cooling in-mold, was mapped onto the initial part CAD geometry and is represented in Figure 4a). These results include a shrinkage correction factor of 15%. Experimental thickness measurements were provided by Agri-Industrial Plastics Company at specific locations on a production tank. These measurements were fitted through all points of the PFT mid-plane mesh using ScanPart, a spline fitting engine provided with the BlowView software package.

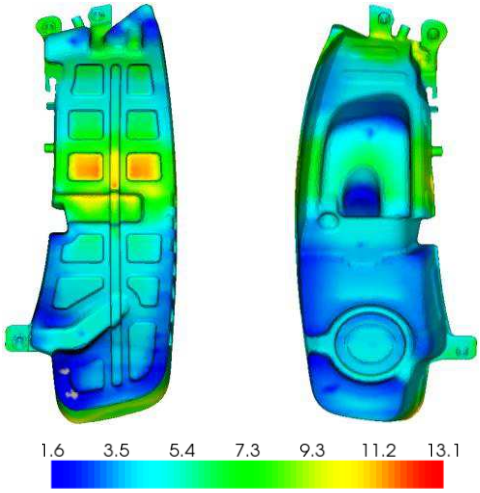

a) BlowView Thickness Prediction (mm)

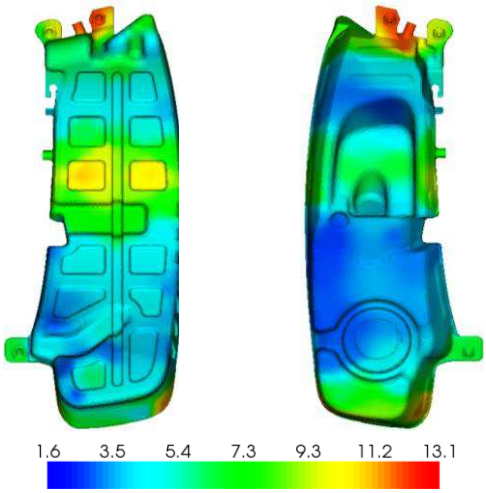

b) Measured Thickness (mm)

Figure 4: Thickness distribution (mm) after mapping on initial part CAD at the end of cooling in-mold

Comparing Figure 4a) and 4b) clearly shows that the predicted thickness results are in good agreement with the experimental data for both the upper and lower shells. Some discrepancies occur in localized areas where the material experiences very high stretch ratios such as on the bottom left and upper right corners of the lower shell, and at the insert location on the upper shell (slightly above the middle). In these areas, BlowView underestimates the thickness. The relative discrepancy is however within 10-15 % error, which is very acceptable considering both the complexity of the part and the forming process.

The warped PFT shape is obtained using BlowView's warpage model, based on the in-mold cooling

conditions given in Table 2, and after being ejected and cooled for 30 minutes in air. The normal distance between the warped PFT and the initial CAD geometry (i.e., ideal part) is computed by aligning the two geometries, using the best fit technique, and is presented in Figure 5. To compare the simulation results to experimental, an engineered scan was provided by Agri-Industrial Plastics Company on a production tank. Using best-fit, the normal distance between the engineered scan and the initial CAD geometry is illustrated in Figure 6. According to the scan measurements, the lateral top and bottom sides of the PFT warp inwards compared to ideal part, whereas the middle warps outwards. Although the same trend is observed in the simulation results, shown in Figure 5, the magnitude of warpage is underestimated. One explanation for this could be related to the differences observed in the predicted wall thickness distribution at certain locations (discussed in the previous section). Secondly, it's important to note that during the in-mold cooling both the heat transfer coefficient and the internal mold wall temperatures are assumed constant. These modelling assumptions may be too restrictive for the warpage simulation and hence contributing to a significant source of error on the predicted temperatures and thermally induced stresses.

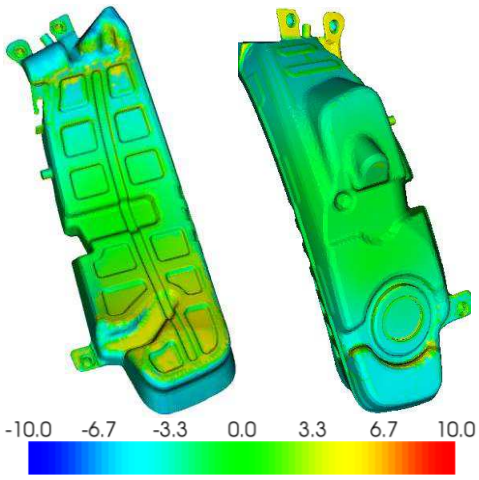

Figure 5: Normal distance (mm) between predicted warped part (simulation) and the initial CAD (ideal part)

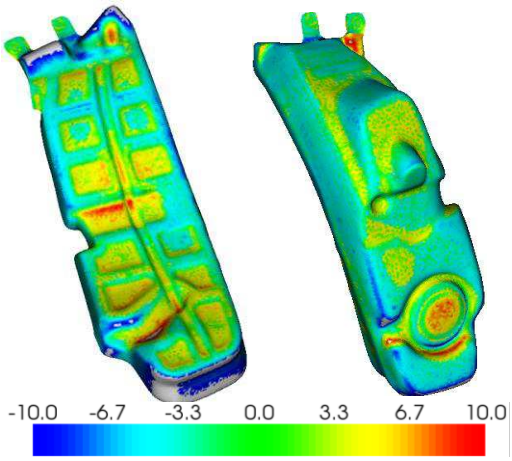

Figure 6: Normal distance (mm) between engineered scan of actual part and the initial CAD (ideal part)

As a final comparison, the predicted warped PFT has been aligned to the engineered scan, according to the best fit technique, and the absolute error deformation (mm) between the two geometries is depicted over the entire shell and reported in Figure 7. These results clearly show that the discrepancy in terms of deformation magnitude (error distances) is between ±8mm. Maximum discrepancies occur in the middle of the lower shell and around the circular insert on the upper shell. Still, the mean error throughout the entire shell is 2.05mm with a standard deviation of 1.75mm.

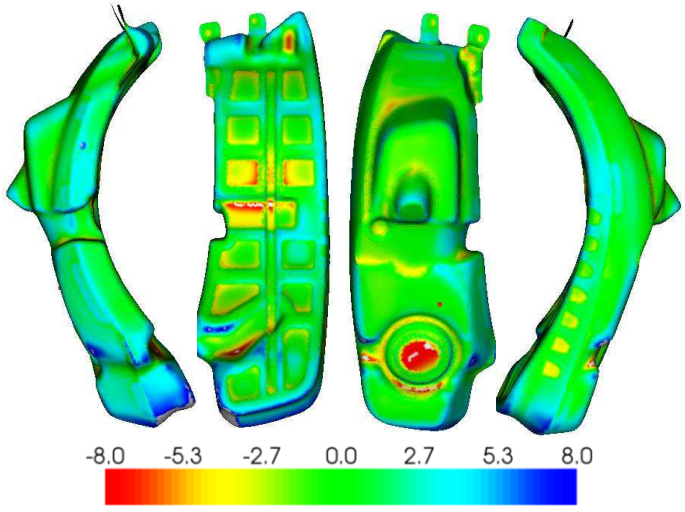

Figure 7: Error distance (mm) between predicted warped PFT (simulation) and engineered scan of actual part (measured)

In order to better evaluate the numerically predicted warpage results to the measurements, a graphical representation is provided in Figure 8, where the error distance is represented along the Y-Z cutting plane at

the center of the part. According to this figure, we can conclude that the predicted warped lower shell deflects outwards for Y<0, and inwards for Y>0, compared to the scanned part. On the other hand, the predicted warped upper shell deflects inwards and outwards along the Y-axis of the scanned part. Furthermore, we observe that the maximum discrepancy between prediction and measurement is approximately -10mm at Y = -230mm on the lower shell, otherwise differences are within ±5mm over the rest of the part along this cutting plane. These results are very acceptable taking into account the part dimension and complex curved shape.

Conclusion

The main focus of this work is to study the warpage deformation during the cooling and solidification of an intermittent extrusion blow molded part. An exhaustive validation study using BlowView's warpage model is presented by comparing simulation results to experimental measurements on an actual PFT. The thermal-mechanical models for the blowing phase and warpage prediction, together with the proposed finite element formulations, has also been recalled. According to this study, it has been demonstrated that the overall accuracy in terms of predicting part thickness, shrinkage and warpage, make BlowView a very suitable simulation tool for industrial design and product development. Future developments will include incorporating the mold cooling channels, in order to improve the part temperature accuracy during the in-mold cooling phase, and thus enhancing the capabilities of this predictive tool.

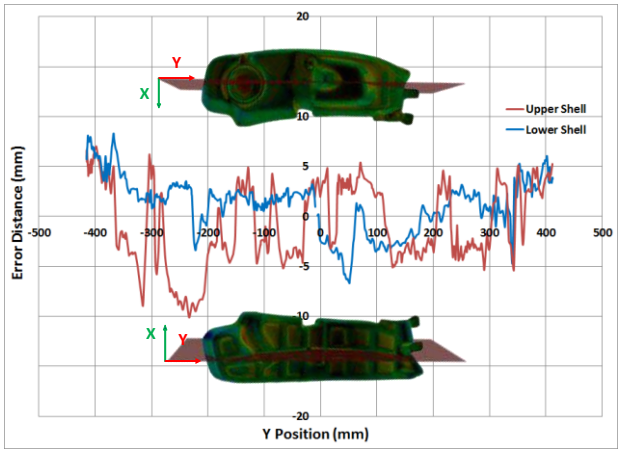

Figure 8: Error distance (mm) between the warped Part CAD (Simulation) and the engineered scan of actual part (Experimental) part on the Y-Z cross section

Table 1: Marlex® HXM 50100 HDPE Material Properties

Young's Modulus (MPa)	437.6
Poisson's ratio	0.47
Maxwell-Weichert relaxation spectrum	
$\bar{g}_k\ (MPa)$	τ_k **(s)**
6.2329260E-02	1.000000E+00
4.0221775E-01	3.659400E+00
2.6434448E-01	3.043196E+02
1.83439170E-01	2.4458976E+04
8.7669350E-02	1.4660196E+07
WLF constants	
T_{ref} **(°C)**	24
C_1	50000
C_2	-211790
Thermo-Physical Constants	
Solidification Temperature (°C)	110
Density at Forming Temperature (kg/m^3)	746
Density at Solid State (kg/m^3)	945

Table 2: Processing Conditions

Mass Flow rate (kg/h)	3733
Extrusion Time (s)	7.0
In-mold Cooling time (s)	180
Tank weight (kg)	3.6
Flash Weight (kg)	3.3

Acknowledgment

The authors would like to acknowledge the NRC-DIGI program for supporting this work, and Agri-Industrial Plastics Company for their contribution in this validation study.

References

1. Debergue P., Massé, H., Thibault, F., Dirrado, R., SAE J. of Materials and Manufacturing, 112 (5), (2004).
2. Massé H., Debergue P., Diraddo R., ANTEC 2004 Congress, Chicago.
3. Debergue P., Massé, H., Thibault, F., Dirrado, R., ESAFORM 2003 Congress, Salerno (Italy).
4. Benrabah Z., Debergue P., Diraddo R., SAE J. of Materials and Manufacturing, 493-501p, (2006).
5. Benrabah Z., Mir H.., Zhang Y., SAE J. of Materials and Manufacturing, 493-501p, (2013).
6. Z. Benrabah, H. Mir, J. Lempicki, A. Bardetti, S. Ahmad, S. Siddiqui, M. Usman, SPE ANTEC Tech. Papers, (2016).
7. Dirrado, R, Plast. Rubber Compos. Process. Appl., 24 (4), 189-196, (1995).
8. Glomsaker, T., Larsen, A., Andreassen, E., Polymer Engineering and Science, 45 (7), 945-952, (2005)
9. Patel, R.M., Sprueill, J.E., Polymer Engineering and Science, 31 (10), 730-738, 1991.
10. Lewis, K. , Morgan, H.R. Thomas, K. N. Seetharamu, The Finite Element Heat and Mass Transfer Analysis, J. Wiley & Sons (1996)
11. Laroche D., Pecora L., DiRaddo R., Puempel A, Savoni L. SPE ANTEC Tech. Papers, (1998).
12. Laroche D., Kabanemi K., Pecora L., DiRaddo R., Polym. Eng. Sci., 39 (7), (1999).
13. Papanastasiou A. C., Scriven L. E., Macosko C. W. J. Rheol. 27, 387-410. (1983).
14. Ferry, J.D., Viscoelastic Properties of Polymers, J. Wiley & Sons (1980)
15. Kaliske M., Robert H., Computational Mechanics 19, 228-239p. (1997)
16. Gu Y., Li H., Advences in Polymer Technologie, Vol 20(1), 14-21, (2001)
17. Yousefi A. M., Doelder J.D., Rainville M.A, Koppi K., Polym. Eng. Sci., 2009 49 (2), 251-263.
18. Yousefi A. M., Atsbha H., Polym. Eng. Sci., 2009 49 (2), 229-239.

CONTACT

Address correspondence to:
Zohir Benrabah, Ph.D.
National Research Council of Canada
Automotive and Surface Transportation Research Centre
Process Modeling Group
75, blvd de Mortagne
Boucherville, Qc, Canada J4B 6Y4
Email : zohir.benrabah@nrc.ca